J Mater Sci (2009) 44:6028–6034
DOI 10.1007/s10853-009-3816-x

Facile fabrication of NiO_xH_y films and their unique electrochromic properties

Fang Liu · Xin Zhang · Kang-Wei Zhu · Yu Song · Zhen-Hua Shi · Bo-Xue Feng

Received: 20 February 2009 / Accepted: 18 August 2009 / Published online: 3 September 2009

Abstract The electrochromic (EC) NiO_xH_y films were fabricated through a facile sol–gel method. The formation of high quality NiO_xH_y films came from adding the xerogel back into the sol and prolonging the annealing time at gradually increasing temperature up to 250 °C. Scanning electron microscopy and atomic force microscopy characterizations indicated films were compact, homogenous, and smooth. Glance angle X-ray diffraction investigation testified NiO_xH_y films were of poor crystallization. The Fourier transform infrared, and thermogravimetry and differential thermal analysis showed that films contained the mixture of NiO, $Ni(OH)_2$, NiOOH, water, and organic substance. With the increasing of the xerogel ratio, the optical absorbance and reflectance of films had larger differences between the colored and bleached state, respectively. The film with the xerogel ratio of 1:5 showed excellent EC properties with a transmittance contrast as high as 60.88% at $\lambda = 560$ nm, which was higher than other sol–gel nickel oxide films reported.

Introduction

The electrochromic (EC) effect is related to a reversible coloration and bleaching process by means of an electrochemical procedure, with simultaneous injection and/or exaction of ions and electrons [1]. As one of EC materials, nickel oxide films capture the attention for their anodic color formation (the color changes from transparent to brown). They can be well paired up with WO_3 of the cathodic color formation to consist of the complementary EC device [2, 3]. Nickel oxide films exhibit soft brown color in the colored state, and can be widely used not only for "smart windows" in buildings, but also in cars, helmets, and information displays [4].

There are many methods to prepare NiO_xH_y films, such as sputtering [5, 6], pulsed laser deposition (PLD) [7], electrodeposition process [8], and sol–gel process [2, 3, 9, 10]. Sputtering and PLD method both need a special machine, while electrodeposition is difficult because of the possible reactions between the semiconductor and solution [6]. Sol–gel method is a facile technique for producing films with lower cost and simple machines. The sol–gel deposition of nickel oxide films is produced by the hydrolysis of nickel (II) alkoxide. However, simple nickel alkoxides are polymeric and insoluble [2], so the most difficult problem is preparing suitable precursors which have sufficient solubility and stability in alcohol solvents [3, 9, 11]. In addition, the nickel oxide film is composed of hydrous nickel oxide, and can be represented as NiO_xH_y film.

In our prior study [12], we have prepared NiO_xH_y films from a simple system, which is composed of nickel acetate tetrahydrate ($Ni(Ac)_2{\cdot}4H_2O$) and polyethylene glycol 6000 (PEG6000) in anhydrous ethanol. We have studied the influence of prepared conditions on the EC properties of NiO_xH_y films. It is found that the concentration of the sol and the annealing process is very important. In this report, the same system was adapted, however, via adding the xerogel back into the sol to increase the concentration of the system. In addition, by prolonging the annealing time at gradually increasing temperature, NiO_xH_y films could be

F. Liu · X. Zhang · K.-W. Zhu · Y. Song · Z.-H. Shi · B.-X. Feng (✉)
Key Laboratory Magnetism and Magnetic Material of Education, Lanzhou University, Lanzhou 730000, People's Republic of China
e-mail: fengbx@lzu.edu.cn

F. Liu
e-mail: liu_f2006@lzu.cn

prepared at 250 °C which is lower than other report [5, 8, 9, 13, 14]. As-prepared films are homogenous without obvious cracks. Films show higher transmission and reflection modulation which is unique for the NiO_xH_y films.

Experiment

Synthesis

All chemicals of analytical grade purity were used without further purification. The precursor solution was prepared by dissolving 0.2 g nickel acetate tetrahydrate ($Ni(Ac)_2{\cdot}4H_2O$) and 0.5 g polyethylene glycol 6000 (PEG6000) in 15 mL anhydrous ethanol. The solution was refluxed for 3 h under continuous stirring around 73 °C. During the reflux, ammonia water was added drop by drop to keep the pH between 8.2 and 8.5, and the solution became blue. The sol was cooled down to room temperature and aged for 1 week.

Some sols were dried in a blasting dry oven at 45 °C until turning into xerogel. The xerogel was added back into a certain amount of sol. The resulting sol was obtained to be blue, transparent, and homogeneous. The resulting sols with different xerogel ratio were denoted as shown in Table 1. The xerogel ratio was defined as the ratio of the sol for preparing the xerogel to that for dissolving the xerogel.

The film was deposited by spin-coating techniques on the indium tin oxide (ITO) transparent conductive substrate (thickness of conducting layer: 180 ± 20 nm; visible transmittance ≥83%, sheet resistance of conducting layer ≤10 Ω) with a size of 2.5 × 2.5 cm^2. The ITO substrates were thoroughly cleaned to wash away any contaminants off the surface. The spin-coating process was operated on the homemade equipment. The spin-coating speed was set at 400, 1000, and 1400 rpm for 30 s, respectively, and the spin-coated film was dried at 120 °C for 10 min. The process was repeated three times. The as-prepared film was pretreated at 120 and 200 °C for 2 h, respectively, then heated at 250 °C for 2 h. The resulting film was transparent and homogenous. It was named as the corresponding sol. The experimental procedure was shown in Fig. 1.

Instrumentations

The surface morphologies were investigated by scanning electron microscopy (SEM, Hitachi S-4800) and atomic force microscopy (AFM, MFP-3D^{TM}). The thicknesses of films were measured by Dektak 8 Advanced Development Profiler. Glance angle X-ray diffraction (GAXRD) was performed on the Philips X' Pert Pro using Cu K_a ($\lambda = 1.54056$ Å) radiation: scan rate of 0.03°/s, glancing angle of 0.5°, scan range of 10–90°.The thermogravimetry (TG) and differential thermal analysis (DTA) were used to analyze the thermal reaction of the xerogel. The xerogels were produced by different $Ni(OH)_2$ sols dried at 45 °C. The samples were denoted as the corresponding sols. The TG–DTA measurements (Diamond TG–DTA PE) were performed under N_2 atmosphere at a heating rate of 10 °C/min in a temperature range of 30–500 °C. The Fourier transform infrared (FTIR, Nicolet NEXUS 670 FT-IR) absorption measurements were obtained by scanned 60 times. The electrochemical redox was carried out in a three-electrode cell on the electrochemistry measuring system (PS-168c). An Ag/AgCl electrode was used as the reference electrode, a platinum wire as the counter-electrode and the resulting film as the working electrode. The electrolyte was the 1 M KOH. Cyclic voltammetries (CV) for the films were performed via triangular wave potential between −300 and 700 mV with a rate of 50 mV/s at the room temperature. The transmittance and reflectance spectra (PERKIN–ELMER Lambda 900 UV/VIS/NIR spectrophotometer) were measured ex situ for the colored and bleached films which were applied pulse potential of +0.7 V (colored) and −0.3 V (bleached) with duration of 45 s, respectively.

Results and discussions

Morphology investigation

Figure 2 shows the SEM images of the A film (the film prepared from the A sol with the 0:1 xerogel ratio, the similar expression adopted in the following). It exhibits a smooth, compact, and highly homogenous surface morphology (Fig. 2a), which is in agreement with reported

Table 1 Xerogel ratio and characteristics parameters for different samples

Sample	Xerogel ratio	Roughness (nm)	Thickness (nm)	Anodic peak potential (mV)	Cathodic peak potential (mV)	Peak potential separation (mV)
A	0:1	2.037	42.7	420	230	190
B	1:5	2.352	48.5	460	220	240
C	1:1	3.010	65.2	490	230	260
D	2:1	5.086	97.4	520	150	360

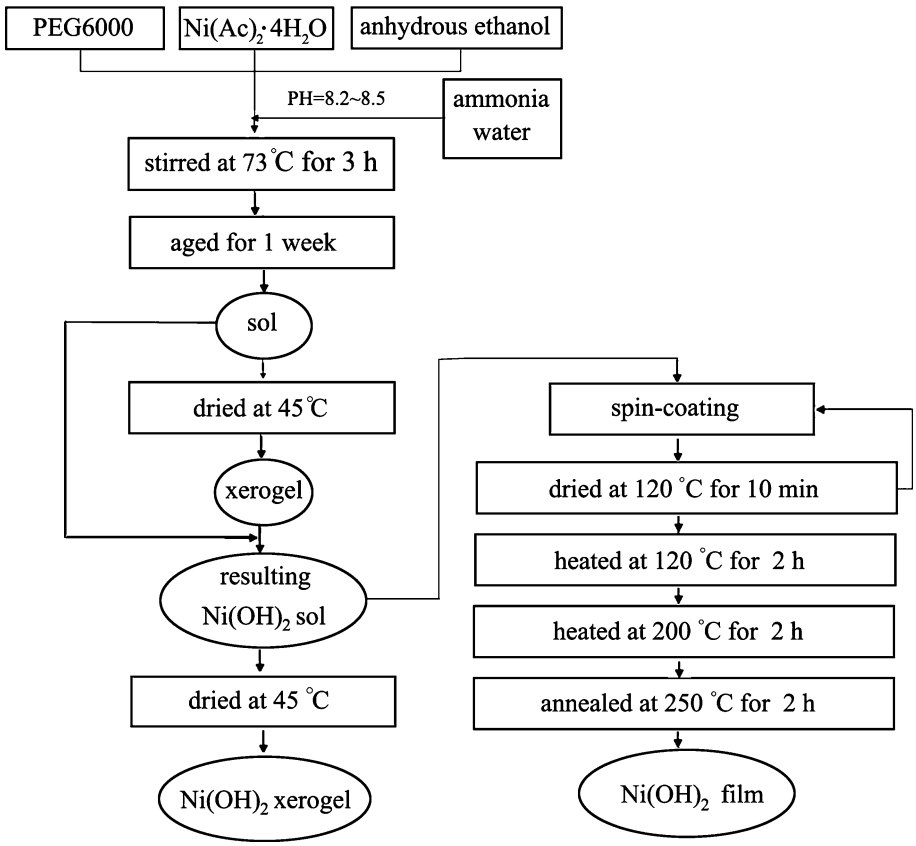

Fig. 1 Schematic procedure for synthesis of NiO_xH_y films with sol–gel method

results [2, 3, 9, 15]. The morphologies of the B, C, and D film have little change (not shown here). The AFM 3D (three dimensional) topography recorded over an area of 20 × 20 μm of the A film is shown in Fig. 3. Although there are many spinous hills on the top of the surface, films are still very smooth. As listed in Table 1, the roughness of NiO_xH_y films is less than 5 nm. The cross section of the A film (Fig. 2b) shows that the thickness is uniform and approximately 40 nm, which accords with the thickness measured by surface profiler shown in Table 1. The film thickness (in Table 1) increases from 40 to 100 nm with the increasing of the xerogel ratio.

Structure analysis

Figure 4 shows GAXRD patterns of NiO_xH_y films on glass substrates. The diffuse peaks between 15 and 35° (2θ) are from the glass substrate. It can be seen that only a low intensity diffraction peak at $2\theta = 44°$ was detected for films annealed at 250 °C, demonstrating the low crystallization of NiO_xH_y species. Although the weak diffraction peak could not be indexed obviously, the XRD curves of some nickel oxide/hydroxide phrases have the strongest peak near 44°, such as Ni_2O_3H (JCPDS, No. 40-1179), $4Ni(OH)_2{\cdot}NiOOH$ (JCPDS, No. 06-0044), $Ni_{1.945}O_3H_{0.815}$ (JCPDS, No. 84-1176), $Ni_{1.94}O_3H_{0.81}$ (JCPDS, No. 78-2343), and $Ni_2O_2(OH)$ (JCPDS, No. 84-1459). As the film was annealed at 400 °C, three diffraction peaks exhibit at $2\theta = 37.08$, 43.35, and 62.82°, which can be indexed as (111), (200), and (220) of the cubic NiO (JCPDS, No. 44-1159).

The FTIR spectroscopy studies were carried out on silicon substrates as shown in Fig. 5. The broad band at 2800–3800 cm^{-1} and the spike at 1620 cm^{-1} are due to the O–H vibration, which corresponds to the existence of the OH^- in water and alcohol [16]. The absorption bands at 2940, 2860, 1650, 1560, 1450, 1410, 740, and 1360 cm^{-1} indicate the presence of the $(–CH_2–)_n$, $–CH_3$, and CH_3COO^- [10, 17]. All of these bands are strengthened with the increase of the xerogel ratio, indicating that there are more organic substances and water staying in films with higher xerogel ratio.

The defined spike at 3680 cm^{-1} corresponds to the antisymmetric stretching of the free hydroxyl groups in the β-$Ni(OH)_2$ [1]. Bands at 522 and 480 cm^{-1} are attributed to the vibration of Ni^{2+}–OH and Ni^{2+}–O from β-$Ni(OH)_2$. The spikes at 660 and 422 cm^{-1} correspond to the vibration of Ni^{2+}–OH and Ni^{2+}–O from α-$Ni(OH)_2$. The bond at 422 cm^{-1} is also a characteristic absorbance for the NiO. The peak near 570 cm^{-1} is due to the O–H stretching vibration of the Ni^{3+}–O stretching vibration, which indicates the existence of the β-NiOOH [18]. It means that

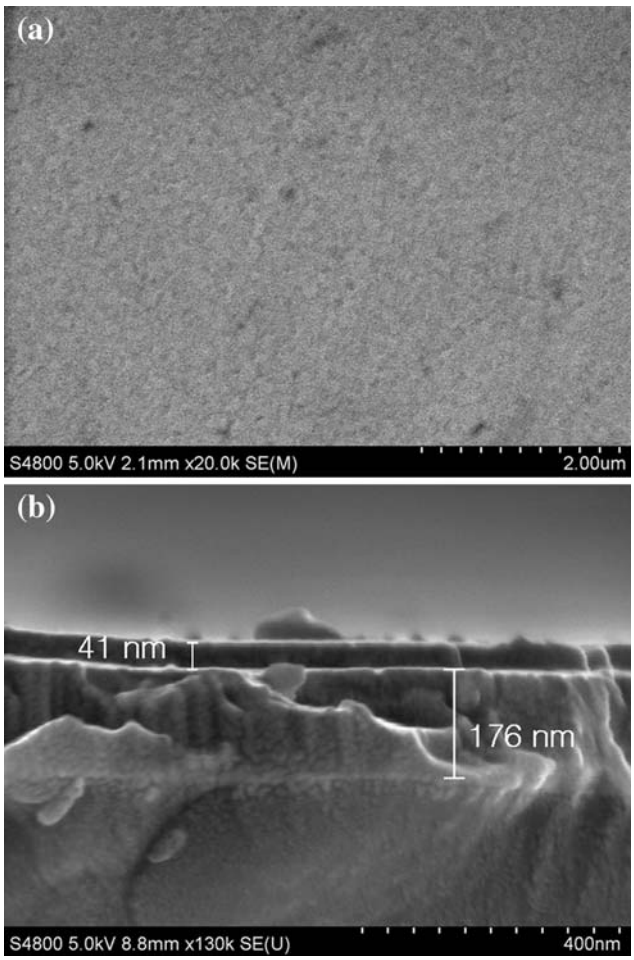

Fig. 2 SEM surface (**a**) and cross-section (**b**) morphologies of the A film on ITO substrate

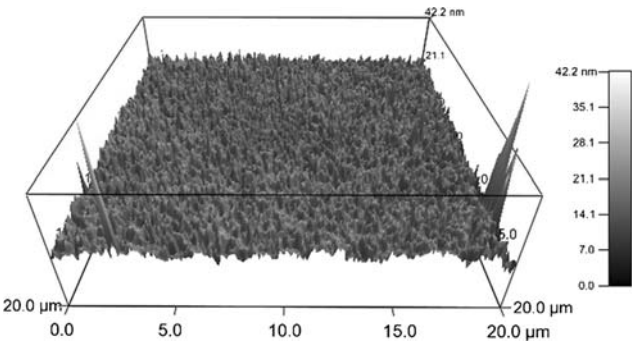

Fig. 3 AFM 3D (three dimensional) images of the A film on ITO substrate

nickel oxide, hydroxide and oxyhydroxide appear in NiO_xH_y films simultaneously, which accords with the low intensity GAXRD peak mentioned above. Cordoba-Torresi et al. [19] have reported similar results and believed that the NiO_xH_y film contained the mixture of the NiO, $Ni(OH)_2$, and NiOOH, but no separated phases of oxide or hydroxide. In addition, all of Ni–O bands exhibit blue shift

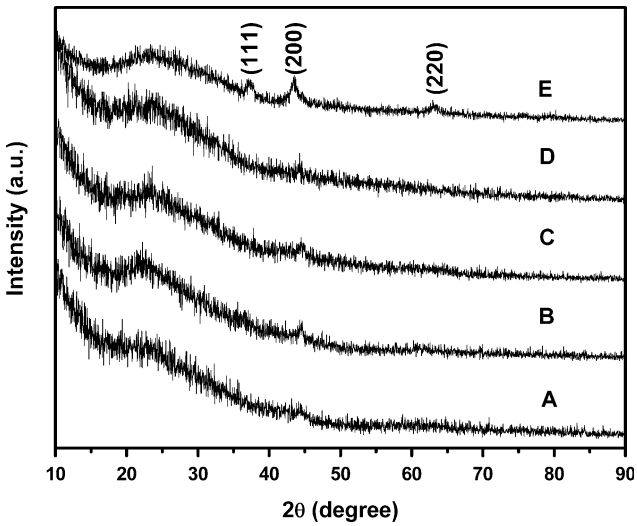

Fig. 4 GAXRD patterns of NiO_xH_y films on glass substrates. Besides the curves for the sample A, B, C, and D, the E curve refers to NiO_xH_y film annealed at 400 °C

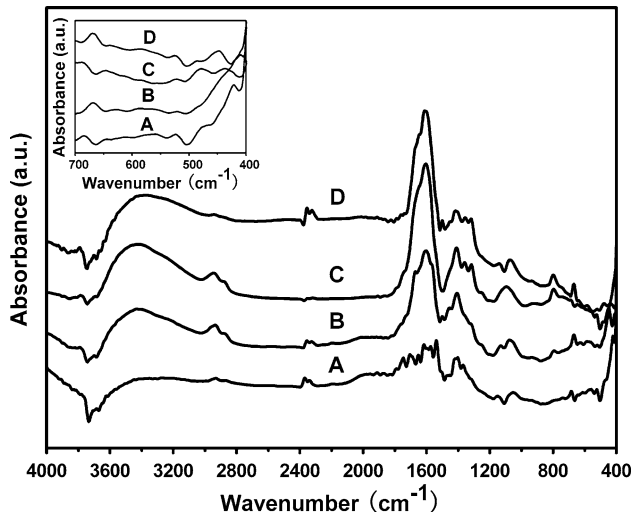

Fig. 5 FTIR subtraction spectra of NiO_xH_y films prepared on silicon substrates. The insert correspond to the range of 700–400 cm^{-1}

with xerogel ratio increases, which may be due to the decrease of the particle size [16, 20].

Thermal analysis

The reactions during the heat treatment were investigated by the xerogel TG–DTA analysis. For the A sample (in Fig. 6a), a small gradual mass loss appears before 280 °C due to the solution venting. An obvious exothermic peak with a 14% mass loss near 300 °C was observed. It corresponds to the decomposition of the crystalline $Ni(OH)_2$. The sharp exothermic peak and the rapid weight loss at 372 °C is related to the decomposition of the amorphous $Ni(OH)_2$ [10, 13, 20, 21] and organic substance. The initial

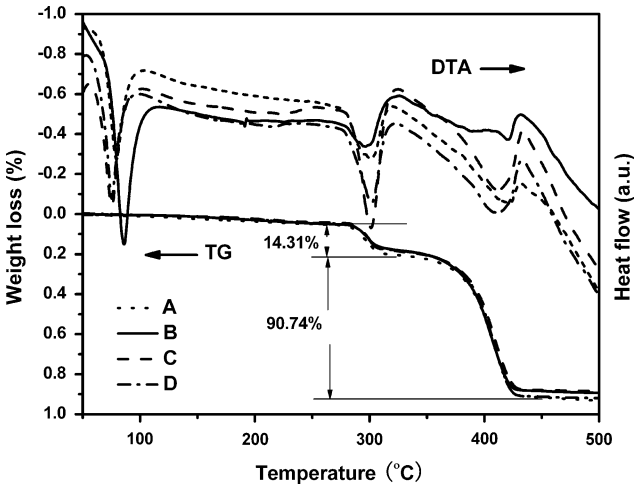

Fig. 6 TG–DTA curves of as-obtained xerogels

mass ratio of the PEG6000 to $Ni(OH)_2$ (reduced from the mass of $Ni(Ac)_2{\cdot}4H_2O$) is 14.9%, which is similar to the 15.7% mass loss ratio between the two mass loss step.

The same chemical process probably occurs during thermal decomposition of the film [22], and the temperature difference between them is around 30–50 °C [17, 23]. In other reports [2, 8], the NiO_xH_y films were always annealed at or above the end temperature of the crystalline $Ni(OH)_2$ decomposition, which is about 300 °C. Herein, for investigating the annealing temperature as low as possible, the films were annealed at 250 °C which is near the onset decomposition temperature of the crystalline $Ni(OH)_2$ phrase. By prolonging the annealing time, the crystalline $Ni(OH)_2$ also can decompose. As a result, the film contains the mixture of NiO, $Ni(OH)_2$, and NiOOH, according to the GAXRD and FTIR analysis. In addition, the annealing progress is composed of 120, 200 and 250 °C, respectively, for 2 h. It makes the solvent venting slow enough to decrease cracks on the surface of films which occur commonly in the sol–gel deposited films. The as-prepared films are compact, homogenous, and smooth without obvious cracks.

For the B xerogel, the onset temperature of the hydrolysis reaction is lower (shown in Fig. 6), hinting the decomposition of crystalline $Ni(OH)_2$ is better than other samples. Besides, it is well-known that in dynamic measurements the decomposition temperature decreases when sample particle size decreases [17, 24]. Therefore, the B film might have smaller grains than other samples.

Electrochromic properties investigation

For the NiO_xH_y films, the coloration/bleaching changes are attributed to oxidative/reductive reaction, with the simultaneous intercalation/deintercalation of ions and electron, which is commonly accepted as following electrochemical reactions [1, 19]:

$$\underset{\text{(bleaching)}}{NiO} + OH^- \leftrightarrow \underset{\text{(coloration)}}{NiOOH} + e^- \quad \text{or} \quad \underset{\text{(bleaching)}}{NiO} + H_2O \leftrightarrow \underset{\text{(coloration)}}{NiOOH} + H^+ + e^- \tag{1}$$

and

$$\underset{\text{(bleaching)}}{Ni(OH)_2} + OH^- \leftrightarrow \underset{\text{(coloration)}}{NiOOH} + H_2O + e^- \text{ or } \underset{\text{(bleaching)}}{Ni(OH)_2} \leftrightarrow \underset{\text{(coloration)}}{NiOOH} + H^+ + e^- \tag{2}$$

Figure 7 shows CVs recorded for different NiO_xH_y films at 10th cycle. The coloration process of the film is associated with the anodic peak appearing before the oxygen evolution reaction (OER), and the bleached process is associated with the cathodic peak. The current densities of the anodic and cathodic peaks increase with the increase in the xerogel ratio, respectively. It implies the increasing of the amount of ions and electrons incorporated into films and the improving of electrochemical reaction activity. The increasing of electrochemical reaction activity is beneficial for the optical absorption modulation of NiO_xH_y films. With the increase of the current densities, the oxidation/reduction peaks shift to higher/lower potentials, leading to a larger potentials separation between the oxidation and reduction peak (listed in Table 1). The increasing trend of potentials separation indicates that the film with higher xerogel ratio has worse reversibility.

As the complementary layers for tungsten oxide films, good reflection modulations of NiO_xH_y films are also in favorable for the unitary transmission modulations of the EC device. As far as we know, there are a few reports on the reflection for nickel oxide films. Herein, the reflectance of NiO_xH_y films was investigated briefly. Figure 8 shows

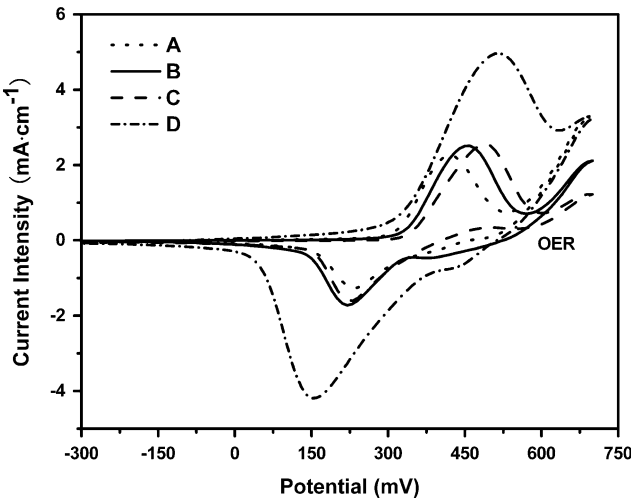

Fig. 7 Cyclic voltammetries of NiO_xH_y films at 10th electrochemical circles

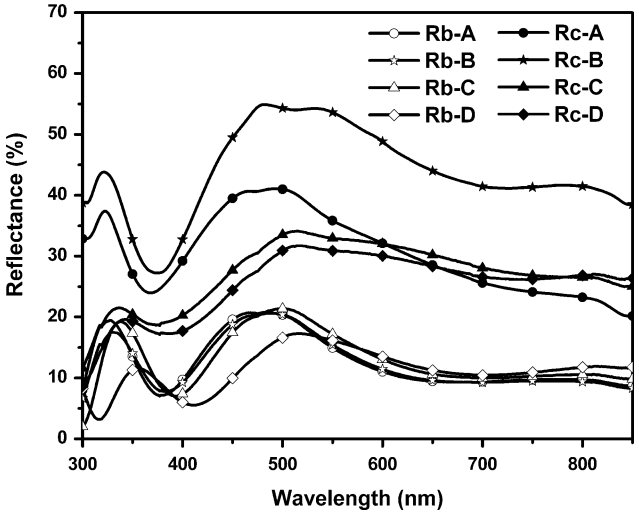

Fig. 8 Optical reflectance spectra of NiO_xH_y films after 10th electrochemical circles

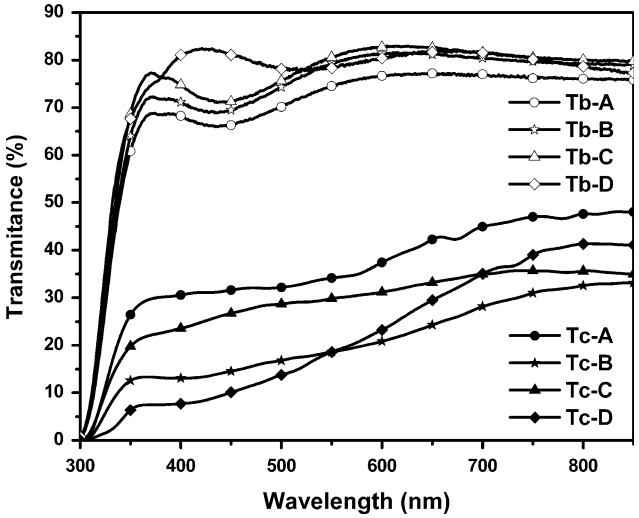

Fig. 9 Optical transmittance spectra of NiO_xH_y films after 10th electrochemical circles

the reflectance of colored (R_c) and bleached (R_b) films after 10th electrochemical circles. R_c is higher than R_b without reference to the xerogel ratio. Granqvist [1] has explained the similar phenomenon for the colored tungsten oxide film as it is caused by electron entering in strongly disordered structure. Herein, NiO_xH_y films are not good crystalline and composed of many components. At the switch of bleached state to colored state, electrons and ions intercalate into films simultaneously. It can be estimated the higher reflectance for colored NiO_xH_y films is due to the same mechanism as tungsten oxide films. Besides, the reflectance decreases with the increasing of the xerogel ratio especially for colored states.

With the increasing xerogel ratio, the film thickness increases, which means that more reactant would take part into the reaction. FTIR analysis has showed that there might be smaller particle size and higher water content for films with higher xerogel ratio. Smaller particle size induces more grain surface and interface as the reaction area for the electrochemical reaction [1]. Cordoba-Torresi et al. [19] have proved that the water staying in the nickel oxide film can not only enhance the reaction rate as the reactant (seen in Eqs. 1 and 2), but also makes many lattice defects to enlarge the active surface and provide the enough channels for the ionic migration. These factors are all favorable for the electrochemical reaction activities, and improve the optical absorption of the colored NiO_xH_y films especially. The reflectance analysis confirms, with the xerogel ratio increased, the R_c decrease and the R_b change a little. Therefore, the optical transmittance for colored states (T_c) decreases with the xerogel ratio increasing, and that for bleached states (T_b) has a little improvement (shown in Fig. 9). Figure 10 shows the optical contrast of the films.

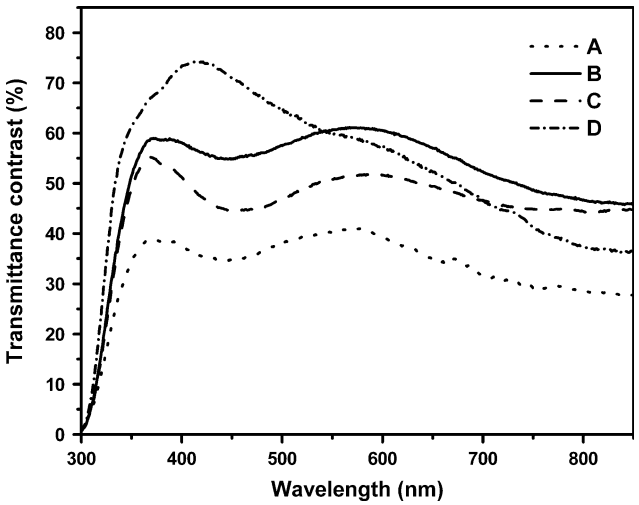

Fig. 10 Optical transmittance contrast of NiO_xH_y films

The D film exhibits best transmittance modulation ability. However, it has only a very short cycling life no more than 20th due to the existence of too much water staying in films which would destroy the electrochemical cycle life and induce the degradation [19].

In addition, TG-DTG investigation has approved that the B film had lower onset decomposition than other films, which means the thermal decomposition completed more sufficiently. As a result, the B film has better modulation ability of visible transmission than any others: at $\lambda = 560$ nm, T_c and T_b are about 18.98 and 79.86%, respectively. The transmittance contrast (ΔT) is high than 60% (shown in Figs. 9 and 10). The ΔT for the sol–gel [3, 8–10], sputter [5], and PLD methods [7] were reported as no higher than 45, 55, and 60%. It means our films have better transmittance modulation.

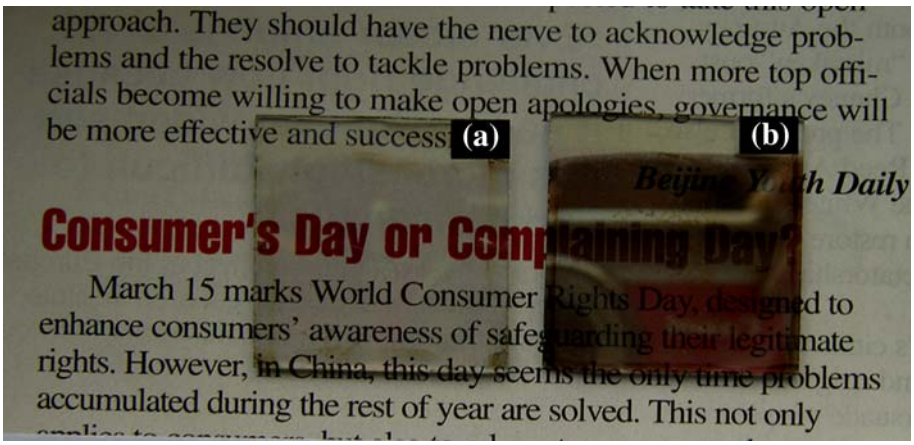

Fig. 11 Photographs of the B film, (**a**) for bleached state and (**b**) for colored state

The colored NiO_xH_y film exhibits brown with a chalceus reflection. As shown in Fig. 11 the reflection for the colored film is so intense that the camera and the finger are clearly seen in the photograph. The phenomena are unique for the EC nickel oxide films and would be beneficial to the unitary transmission modulations of the EC device.

Conclusions

The unique EC NiO_xH_y films were fabricated through a facile sol–gel method. The NiO_xH_y films can be prepared at 250 °C via prolonging the annealed time at gradually increasing temperature. By adding the xerogel back into the sol, the concentration of sol can be increased notably. And the thickness of the corresponding film increases. SEM and AFM morphologies show the NiO_xH_y films are compact, homogenous and smooth. The TG–DTA, FTIR, and GAXRD analysis show that nickel oxide films contain the mixture of the NiO, $Ni(OH)_2$, NiOOH, water, and some organic substance, but no separated phases of oxide and hydroxide co-exists. With the increasing of the xerogel ratio, the amount of the organic substance and water staying in the film increases, while the particle size decreases. The optical reflectance of films shows a large difference between the colored and bleached state, which is favorable for transmission modulation properties accompanied with absorbance. The film with the xerogel ratio of 1:5 shows good EC properties whose ΔT is as high as 60.88% at $\lambda = 560$ nm, which is higher than other nickel oxide films prepared by sol–gel method.

Acknowledgement We appreciate the financial supports of the National science Foundation of China (Grant No. 60576013, 60536010 and J0630313).

References

1. Granqvist CG (1995) Handbook of inorganic electrochromic materials. Elsevier, Amsterdam
2. Garcia-Miquel JL, Zhang Q, Allen SJ, Rougier A, Blyr A, Davies HO, Jones AC, Leedham TJ, Williams PA, Impey SA (2003) Thin Solid Films 424:165
3. Ozkan Zayima E, Turhan I, Tepehan FZ, Ozer N (2008) Sol Energy Mater Sol Cells 92:164
4. Granqvist CG (2006) Nature 5:89
5. Liu H-R, Zheng W-M, Yan X, Feng B-X (2008) J Alloys Compd 462:356
6. MiIIer EL, Rocheleau RE (1997) J Electrochem Soc 144:1995
7. Bouessay I, Rougier A, Tarascon J-M (2004) J Electrochem Soc 151:H145
8. Wu M-S, Yang C-H (2007) Appl Phys Lett 91:033109
9. Xia XH, Tua JP, Zhang J, Wang XL, Zhang WK, Huang H (2008) Electrochim Acta 53:5721
10. Sharma PK, Fantini MCA, Gorenstein A (1998) Solid State Ionics 113–115:457
11. Moser FH, Lyman NR (1990) US Patent No. 4959247, 25 September
12. Liu F, Zhou M, Zhong Y-Y, Song Y, Li J-R, Yang W-F, Feng B-X (2008) J Funct Mater 39:1835
13. Xia XH, Tu JP, Zhang J, Wang XL, Zhang WK, Huang H (2008) Sol Energy Mater Sol Cells 92:628
14. Lin S-H, Chen F-R, Kai J-J (2008) Appl Surf Sci 254:2017
15. Ryu HW, Choi GP, Lee WS, Park JS (2004) J Mater Sci 39:4375. doi:10.1023/B:JMSC.0000033431.52659.e5
16. Liu X-M, Zhang X-G, Fu S-Y (2006) Mater Res Bull 41:620
17. Cerc Korošec R, Šauta Ogorevc J, Draškovič P, Dražić G, Bukovec P (2008) Thin Solid Films 516:8264
18. Šurca A, Orel B, Pihlar B, Bukovec P (1996) J Electroanal Chem 40:83
19. Cordoba-Torresi SI, Hugot-Le Goff A, Joiret S (1991) J Electrochem Soc 138:1554
20. Cerc Korošec R, Bukovec P (2004) Thermochim Acta 410:65
21. Cheng J, Cao G-P, Yang Y-S (2006) J Power Sources 159:734
22. Cerc Korošec R, Bukovec P, Pihlar B, Padežnik Gomilšek J (2003) Thermochim Acta 402:57
23. Cerc Korošec R, Bukovec P (2006) Acta Chim Slov 53:136
24. Wendlandt WW (1964) Thermal methods of analysis. Interscience Publishers, New York, p 17